

# Normal-mode matching localization in shallow water: Environmental and system effects

S. M. Jesus

SACLANT Undersea Research Centre, Viale San Bartolomeo 400, I-19026 La Spezia, Italy

(Received 2 March 1990; revised 8 January 1991; accepted 5 June 1991)

Matched-field processing is a passive range and depth source localization technique that has been extensively used in shallow-water environments. A vertical array of sensors is used to spatially sample the acoustic waveguide where the source signal embedded in additive ambient noise propagates. The array output is then matched with the signal replica field generated by a normal-mode model based on the environmental parameters that characterize the waveguide. Recent results obtained from real data show the feasibility of the technique and give evidence of its strong dependence both on the array aperture and on the knowledge of the environmental parameters used in the model. This paper describes a modified matched-field technique, called normal-mode matching, that is applied to real shallow-water data. Its performance is compared to that obtained by conventional matched-field processing using the same data set. Unlike conventional matched-field processing, the results indicate that unambiguous localizations can be obtained even for "short" arrays spanning only half of the water column.

PACS numbers: 43.30.Bp, 43.30.Wi

## INTRODUCTION

Passive range and depth localization of an acoustic source in shallow water is a difficult, yet interesting problem that has received a great deal of attention in the last few years.<sup>1-5</sup> The simultaneous estimation of range and depth requires the use of numerical propagation models. The classical approach to this problem is to "match" the received acoustic data with the sound field predicted by the propagation model for a number of hypothetical range/depth source locations. This technique is called *matched-field processing*.

It is commonly accepted that the wave propagation and boundary interaction dominating shallow-water propagation can be well described by a normal-mode model. According to this model, the acoustic pressure measured at the receiver can be expressed as a linear combination of the natural modes (or normal modes) of vibration of the waveguide. The complex weights associated with the normal-mode depth functions of the waveguide, herein designated as normal-mode amplitudes, fully characterize the source-medium interaction and contain the source location information. Recently, techniques have been suggested that use the normal-mode amplitudes to extract the source location parameters, source depth,<sup>6</sup> and source range.<sup>7</sup> A unified framework allowing simultaneous estimation of source range and depth proposed by Yang<sup>8</sup> has been used in a very similar fashion by Wilson *et al.*<sup>9</sup> Modified versions of this technique have also been proposed recently by Smith *et al.*<sup>5</sup> and Shang.<sup>10</sup> This technique uses the linearity of the normal-mode propagation model to perform a change of variables from the cylindrical range coordinates to the normal-mode space coordinates. The idea pursued is to measure the degree of similarity between the estimated and the model-generated normal-mode amplitudes. The maximum of the similarity function will give an estimate of the range/depth source parameters.

also called matched-mode processing. Yang<sup>8</sup> derived range and depth estimation patterns from simulated data and successfully applied the method to experimental data obtained from a long-range source signal propagation in the Arctic surf duct. In studies by Yang<sup>8</sup> and Wilson *et al.*,<sup>9</sup> the sound field was unresolvable by the receiving array; i.e., there were more modes than sensors, but the array still spanned a large portion of the sound channel. Other studies<sup>5,10</sup> emphasized range/depth estimator detection and resolution performances.

The present study examines the real data performance of the normal-mode matching technique in a shallow-water environment. The results are compared to those obtained by conventional matched-field processing in the same data set. Particular emphasis is made on the array geometry, source depth, source frequency and bottom characteristics.

## 1. THEORY

The ocean environment is modeled as a stratified waveguide with an arbitrary sound-speed profile in the vertical. Long-range sound transmission in such an environment can be described by the discrete normal-mode model.<sup>11</sup> Given the acoustic pressure predicted by a sufficiently accurate propagation model, range/depth estimation of a submerged source is an inverse problem. The impossibility of obtaining a numerical or analytical inverse solution make us resort to approximate solutions by forward modeling predictive techniques. Matched-field processing belongs to this category of forward modeling techniques. Matched-field processing can be viewed as a two-dimensional (range and depth) generalized beamformer; each "steering" vector is the model replica field formed by the point solution to the wave equation that describes the propagation between the source and the receiver for a given "look direction" in the range/depth space.

an "infinite" number of source range/depth combinations gives rise to an ambiguity surface. The coordinates of the maximum of this surface are the matched-field estimates of the actual range and depth source location. Normal-mode matching proceeds by direct inversion of the propagation model in order to estimate the normal-mode amplitudes. Forward modeling is then applied to estimate the source parameters by matching the estimated and the model predicted normal-mode amplitudes for a number of source range/depth combinations. Again, the range/depth coordinates of the maximum level of the ambiguity surface obtained gives the normal-mode matching estimate of the source location.

### Normal-mode modeling

The solution of the wave equation for a narrow-band point source exciting a horizontally stratified, parallel waveguide is commonly expressed as a linear combination of the waveguide normal-mode depth functions. The normalized spatial dependence of the acoustic pressure measured at a vertical array of  $L$  sensors due to a unit power narrow-band source at location  $\theta_T^t = (z_T, r_T)$ , where superscript  $t$  stands for transpose and subscript  $T$  indicates the true source location, may be expressed as<sup>11</sup>

$$\mathbf{p}(\theta_T) = \mathbf{A}\mathbf{x}(\theta_T), \quad (1)$$

where  $\mathbf{p}(\theta_T)$  is the  $L$ -dimensional vector of array output pressures,  $\mathbf{A}$  is an  $L \times M$  real matrix whose columns are the normal-mode depth functions expressed for all sensor depths  $\{z_l; l = 1, \dots, L\}$ ,

$$\mathbf{A} = [\mathbf{a}_1, \mathbf{a}_2, \dots, \mathbf{a}_M], \quad (2a)$$

where

$$\mathbf{a}_m^t = [a_m(z_1), a_m(z_2), \dots, a_m(z_L)] \quad (2b)$$

and  $M$  is the number of modes supported by the waveguide. The  $M$ -dimensional complex vector  $\mathbf{x}(\theta_T)$  is the normal-mode amplitude vector for the true source parameter location,  $\theta_T$ , the  $m$ th element of which is defined by

$$x_m(\theta_T) = [a_m(z_T)/\sqrt{k_m}] e^{-\alpha_m r_T} e^{ik_m r_T}, \quad (3)$$

where  $\alpha_m$  is the  $m$ th mode attenuation coefficient. The two sets  $\{a_m(z); m = 1, \dots, M; 0 < z < H\}$  and  $\{k_m; m = 1, \dots, M\}$  are the mode depth functions and the corresponding mode horizontal wave numbers characterizing the propagation channel of depth  $H$ . Note that these expressions have been obtained by normalizing out the range dependence, a phase shift and an arbitrary constant. The SACLANTCEN normal-mode model, SNAP,<sup>12</sup> is a computer program well-suited for calculating the acoustical pressure defined in (1). SNAP has been used in this study to calculate the mode depth functions, the corresponding horizontal wavenumbers and mode attenuations.

### Normal-mode amplitude estimation

Assuming that the acoustical pressure  $\mathbf{p}(\theta_T)$  is corrupted by additive zero-mean Gaussian noise  $\epsilon_p$ ,

$$\mathbf{y}(\theta_T) = \mathbf{p}(\theta_T) + \epsilon_p, \quad (4)$$

$$\hat{\mathbf{x}}(\theta_T) = [\mathbf{A}^t \mathbf{R}_{\epsilon_p}^{-1} \mathbf{A}]^{-1} \mathbf{A}^t \mathbf{R}_{\epsilon_p}^{-1} \mathbf{y}(\theta_T), \quad (5)$$

where the noise and the acoustical pressure are assumed uncorrelated and  $\mathbf{R}_{\epsilon_p} = E\{\epsilon_p \epsilon_p^t\}$  is the noise covariance matrix. In practice, the white noise assumption reduces (5) to  $\hat{\mathbf{x}}(\theta_T) = [\mathbf{A}^t \mathbf{A}]^{-1} \mathbf{A}^t \mathbf{y}(\theta_T)$ , which requires the inverse of  $\mathbf{A}^t \mathbf{A}$ , i.e., requires matrix  $\mathbf{A}$  to be full rank. If  $\mathbf{A}$  is a rank deficient matrix (our case),  $r(\mathbf{A}) = k$  with  $k < \min(L, M)$ , then  $\hat{\mathbf{x}}(\theta_T)$  is not unique and the optimal least-squares solution of (1) is

$$\hat{\mathbf{x}}(\theta_T) = \mathbf{A}^+ \mathbf{y}(\theta_T), \quad (6)$$

where  $\mathbf{A}^+$  is the pseudo-inverse of  $\mathbf{A}$ . Equation (6) is also referred to as the minimum (Euclidean) length solution of (1).<sup>13</sup>

### C. Source range/depth estimation

The approximate forward solution to the inverse problem is obtained as the range/depth coordinates for which the direct match between the measured and the model predicted quantities is maximum. For the normal-mode matching (NMM) technique, this is written as

$$RD_{\text{NMM}}(\theta) = E\{|\hat{\mathbf{x}}^H(\theta_T) \mathbf{w}(\theta)|^2\}, \quad (7)$$

where  $\mathbf{w}(\theta)$  is the model replica normal-mode amplitude vector at the source location  $\theta$ . In the expression of  $\mathbf{w}(\theta)$  given by (3), the compressional-wave attenuation coefficient  $\exp(-\alpha_m r_T)$  has been dropped as suggested by Yang<sup>8</sup> and confirmed by our own tests in our shallow-water environment.

A similar expression is obtained for the conventional matched-field processor (MFP),

$$RD_{\text{MFP}}(\theta) = E\{|\hat{\mathbf{y}}^H(\theta_T) \mathbf{p}(\theta)|^2\}, \quad (8)$$

where  $\mathbf{y}$  and  $\mathbf{p}$  have been defined above. If the sound field is correctly sampled, i.e., if the array is sufficiently dense to resolve even the higher-order modes and it spans the significant part of the sound channel, matrix  $\mathbf{A}$  will be column orthonormal in which case, (7) and (8) will be equivalent. In that case, (7), or (8), will be the optimum receiver of single point source in white noise. In practice, the spatial observation of the sound field is often restricted to some imperfectly, spatially sampled portion of the water column. This and the fact that in shallow water a large amount of energy is often lost by bottom-sound wave interaction result in a rank deficiency of matrix  $\mathbf{A}$ . Thus expression (6) must be used as the normal-mode amplitude estimator. By substituting (6) into (7) and using (1), this estimator gives the normal-mode matching processor response of the form

$$RD_{\text{NMM}}(\theta) = E\{|\mathbf{x}^H(\theta_T) \mathbf{V}_k \mathbf{V}_k^t \mathbf{w}(\theta) + \epsilon_p^H [\mathbf{A}^+]^t \mathbf{w}(\theta)|^2\}, \quad (9)$$

where the decomposition  $\mathbf{A} = \mathbf{U} \mathbf{\Sigma} \mathbf{V}^t$  has been used and where  $\mathbf{V}_k$  is a  $M \times k$  eigenvector matrix corresponding to the  $k$  largest singular values of  $\mathbf{A}$ . Reducing the number of normal modes improves the quality of the match, since the modes that have been rejected are those having the largest estimator variance [smallest eigenvalues of the covariance matrix of the maximum-likelihood estimator (5)]. The

by Yang<sup>8</sup> and solved in an subjective way by rejecting the smaller eigenvalues of an augmented version of matrix  $A'A$ . In this case, the  $k$  modes being selected are not necessarily the  $k$  lower-order modes but are the most energetic modes that are resolvable by the array. The way normal-mode matching adapts to the array configuration contrasts with conventional matched-field processing where the replica acoustic pressure is computed for all the scan source locations using all the modes, regardless of the array configuration. As we will see below, this difference will have a strong impact on the estimated range/depth ambiguity surface for many practical situations and in particular in shallow waters.

# I. REAL DATA RESULTS

Real data have been acquired in the area north of Elba (island off the west coast of Italy). This area is characterized by a water depth of 118 to 125 m above a sandy bottom formed by a 2.5-m-thick medium/hard sediment layer and a semi-infinite homogeneous subbottom (Fig. 1). The water sound-speed profile (see Fig. 1) is the typical September–October Mediterranean downward refracting profile with a high-temperature surface layer extending to 40-m depth. The environmental model described above and the corresponding bottom parameters have been established in Ref. 14. The receiving system was a free-drifting 62-m-long vertical array with 64 unequally spaced hydrophones (Table I) with the uppermost hydrophone situated at depth of about 40 m. The signal was simulated by an acoustic sound source emitting a continuous wave tone at one of the following frequencies: 180, 332, or 740 Hz. The source was stationed at either 6 or 71 m, or was towed by an auxiliary ship at a depth of approximately 61 m. Ranges between the source and the receiving array varied from 5 to 27 km. The signals received at the array were transmitted via a high-density radio link to the ship. After sampling at a rate of 4000 Hz, all the 64 channels were fast Fourier transformed with a block size of 1024 samples. The interval between each time snapshot was approximately 1.5 s due to the time needed for processing. Three frequency bins, 4 Hz apart, in the neighborhood of the source frequency were saved for each time snapshot. An approximate array-averaged signal + noise-to-noise ratio was

TABLE I. Vertical array configuration.

Hydrophone no.		Spacing (m)
From	To	
1	8	2
8	16	1
16	48	0.5
48	56	1
56	64	2

estimated by comparing the power received at the source frequency to that received on a contiguous frequency bin. This value was of the order of 20 to 30 dB.

The real data set acquired in the area north of Elba consists of more than 12 h during a 3-day period. From the three source frequencies (180, 332, 740 Hz) only 332 Hz gave acceptable results. Occasionally accurate results could be obtained at 740 Hz for the deep source locations (61 and 71 m) and short ranges (< 10 km); in these cases the source localization was very unstable (in time) and the sidelobe rejection (i.e., the difference, in dB, between the maximum and the highest sidelobe in the surface) was very low. At 332 Hz, a 20-min period of relatively stable results was obtained at the end of a tow at 5-to 7-km range. Figure 2, extracted from that 20-min-period, shows two range/depth ambiguity surfaces obtained from the match of the complete set of modes supported by the channel. Figure 2(a) (simulated data) shows a sharp peak at the correct source location with a sidelobe rejection of 3.5 dB and a relatively small sidelobe

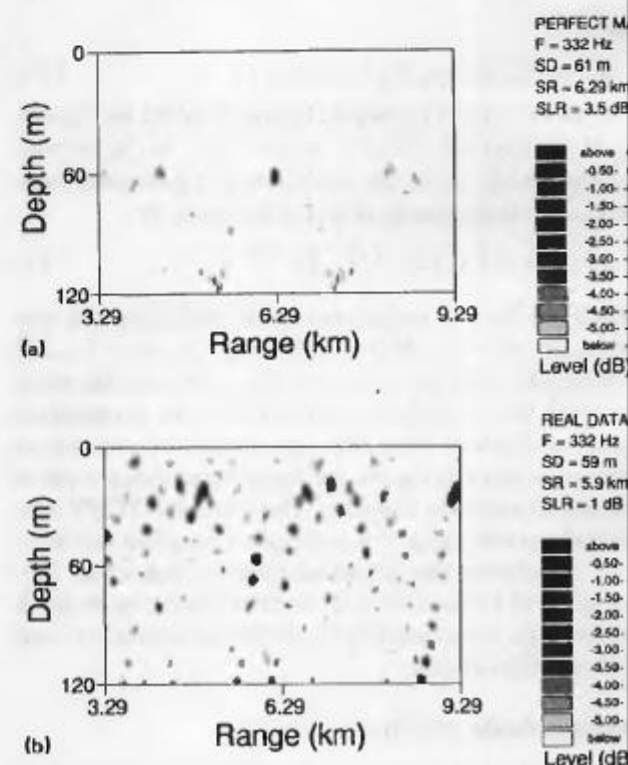
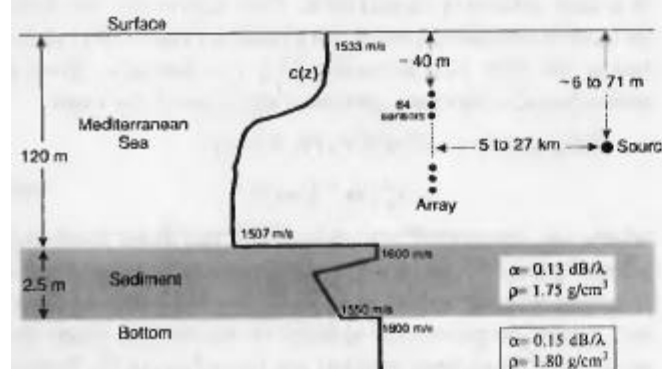


FIG. 2. Range/depth ambiguity surfaces in the scenario of Fig. 1. Exp



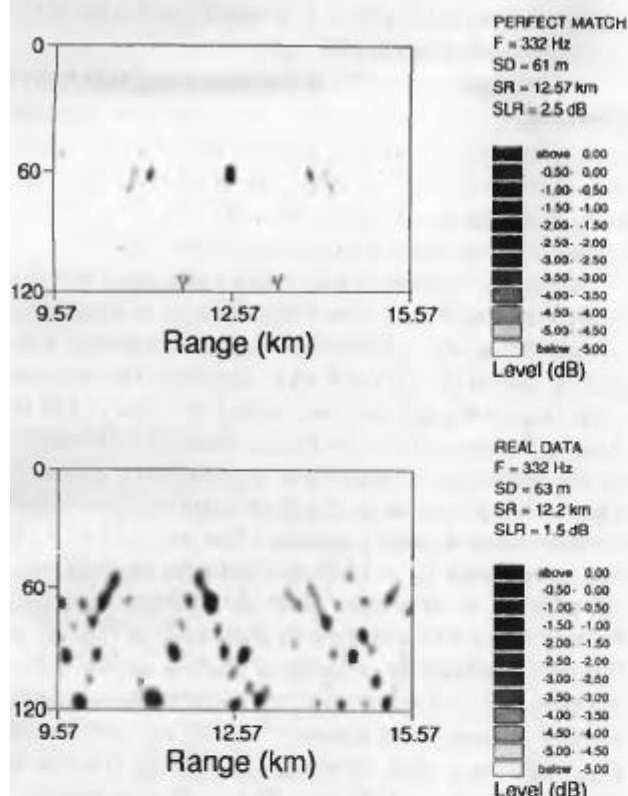


FIG. 3. Range/depth ambiguity surfaces in the scenario of Fig. 1. Expected source depth/range is 61 m/12.57 km; perfect match with simulated data and real data (b) where estimated source depth/range is 63 m/12.2 km.

average concentrated below the thermocline (depth > 40 m). This is in contrast with the real-data range/depth ambiguity surface [Fig. 2(b)], which shows a large number of lobes (even above the thermocline) with levels up to 1 dB below the maximum. The maximum is obtained for a source located at 59-m depth and 5.9-km range. This is very close to the expected values (61 m and 6.29 km).

Most parts of the other runs were made at longer ranges, from 10–25 km. Figure 3 shows one occasional result obtained at a range of 12.5 km and for a source depth of 61 m. The range/depth surface of Fig. 3(a) (simulated data) is similar to that of Fig. 2(a), however, it shows some higher lobes up to 2.5 dB below the maximum, due to the longer range of propagation. Figure 3(b) (real data) shows a precisely located source with a sidelobe rejection of 1.5 dB and a very small range-depth estimation error of 3% both in depth and in range. Note here, however, that in contrast to the result of Fig. 2(b), no significant sidelobes appear above the thermocline, considerably reducing the surface ambiguity. This reduction is due to the fact that only a reduced number of modes have been used for the range/depth match: 8 modes out of the 17 supported by the channel.

## DISCUSSION

The real data performance of the normal-mode matching processor will be discussed on the basis of simulated data and results obtained in the same source-medium-receiver condi-

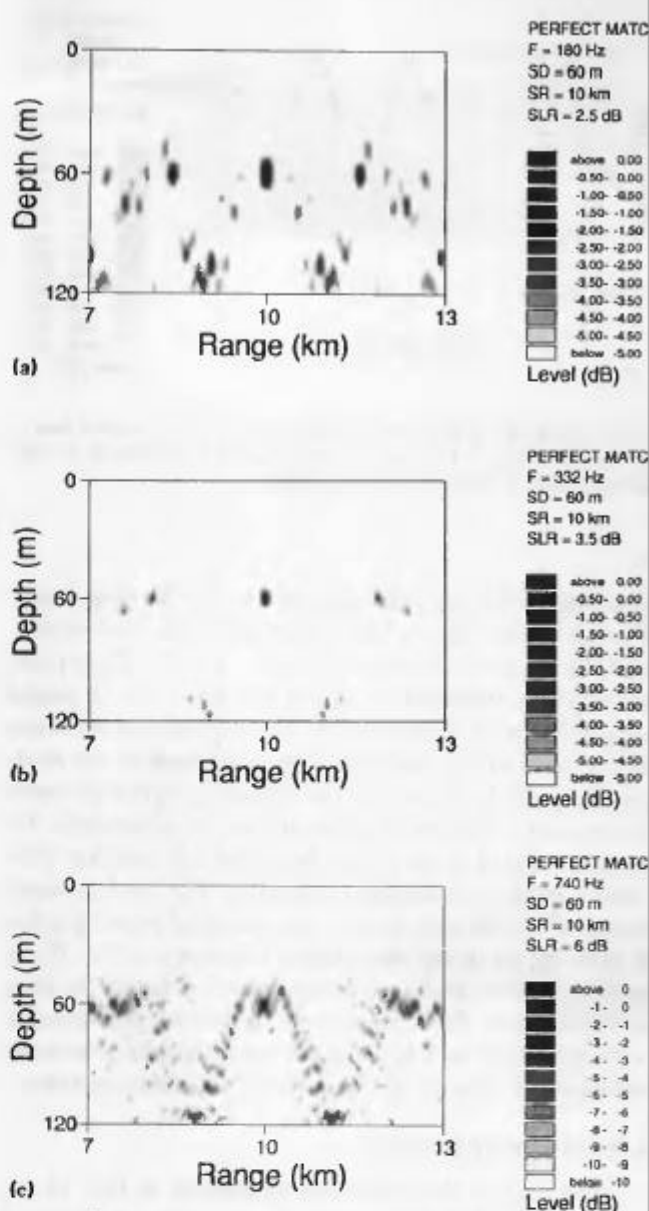


FIG. 4. Range/depth ambiguity surfaces obtained from simulated data in the scenario of Fig. 1. Source depth/range is 60 m/10 km: at (a) 180 Hz, (b) 332 Hz, and (c) 740 Hz.

environment and receiver mismatch tests. Comparison is made with the performance and robustness of the matched field processor in the same conditions.

Before starting the discussion of each particular environment or system parameter, let us look at the expected performance of the normal-mode matching processor in the real source-medium-receiver conditions free of both noise and mismatch. For this test, two source depths were selected: a shallow source at 6 m and a deep source at 60 m. A mean range of 10 km was chosen for this test. The results obtained for the three source frequencies are shown in Fig. 4. At 180 Hz only nine modes exist, which results in a small sidelobe rejection of 1 dB for the shallow source (not shown) and 2.5 dB for the deep source [Fig. 4(a)]. At 332 Hz [Fig.

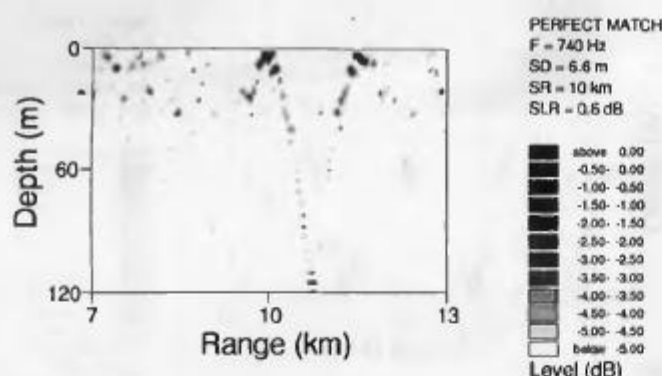


FIG. 5. Range/depth ambiguity surfaces obtained from simulated data in the scenario of Fig. 1. True source depth/range of 6 m/10 km at 740 Hz. Estimated source depth/range is 6.6 m/10 km.

increased to 3.5 and 6 dB respectively, for the deep source position (60 m). Severe localization problems were encountered for the shallow source at 740 Hz (Fig. 5). These problems can be explained by noting that from the 38 modes supported by the channel at 740 Hz only the first 30 modes can be resolved by the array (estimated rank of the mode depth matrix  $\mathbf{A}$ ). However, the remaining eight high-order modes carry a non-negligible amount of information for sources situated in the surface layer and it is therefore difficult to obtain a reasonable localization. For the 6-m depth source at 332 Hz (not shown), the estimated source depth is in error by 0.6 m and the sidelobe rejection is of 3.5 dB. In general, the best results were obtained at 332 Hz for the deep source location. The assessment of the relative performance of the normal-mode matching and matched-field processors using the real data set of Fig. 2 follow in the next sections.

#### A. Environmental effects

The bottom characteristics established in Ref. 14 assume a 2.5-m-thick fluid sediment with density  $1.75 \text{ g/cm}^3$  and compressional-wave attenuation of  $0.13 \text{ dB}/\lambda$ . The sound speed in the sediment varies from 1530 to 1600 m/s. The subbottom has a slightly higher density ( $1.8 \text{ g/cm}^3$ ) and

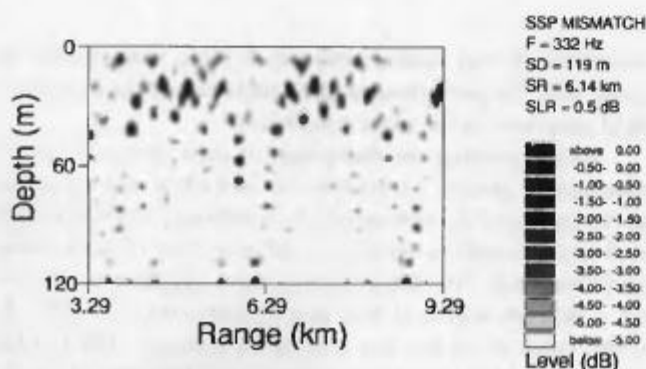


FIG. 6. Range/depth ambiguity surfaces obtained from simulated data in the scenario of Fig. 1 with subbottom sound speed mismatch: true 1800

an attenuation of  $0.15 \text{ dB}/\lambda$ . The sound speed in the sediment is assumed equal to 1600 m/s.

In previous studies,<sup>4,15</sup> it was mentioned that both normal-mode matching and the matched-field processor were relatively insensitive to mismatches on bottom properties. This conclusion was based on simulated tests with an array of sensors spanning the total 120-m water column and a sound source emitting a continuous wave at 740 Hz.

Using the scenario of Fig. 1, and a frequency of 332 Hz it has been found that even small changes in some bottom parameters could significantly degrade the result. This is mainly due to the reduced array aperture, the downward refracting profile and the lower source frequency (332 Hz). Among the several tests, the results obtained with mismatches on the subbottom sound speed is particularly interesting. Figure 6 shows the range/depth ambiguity surface obtained from the normal-mode matching of the true field with a subbottom sound speed  $C_b = 1800 \text{ m/s}$  and a replica field generated with  $C_b = 1600 \text{ m/s}$ . Note the striking resemblance between this result and the real data result of Fig. 2(b). In this case, the sidelobe coverage at shallow depths is due to the bottom sound speed mismatch which results in a number of unresolved modes: 17 modes are assumed with  $C_b = 1600 \text{ m/s}$  while 29 modes do exist on the true bottom obtained with  $C_b = 1800 \text{ m/s}$ . The result of processing a real data record of Fig. 2(b) with  $C_b = 1700 \text{ m/s}$  is shown in Fig. 7. The sound source is unambiguously located with sidelobe rejection greater than 1 dB at 56-m depth and 6.29 km range. The overall aspect of the range/depth surface obtained in this case is much closer to that expected from the perfect match case [Fig. 2(a)]. Changes in other environmental parameters such as water depth and bottom attenuation, showed no improvement.

#### B. System effects

In Fig. 2(a) and (b), the source location is precisely pinpointed. This high resolution indicates that a relatively high number of accurately estimated modes were used in the match process. However, Fig. 2(b) exhibits a number of high-level sidelobes at shallow depths that are absent in the perfect match case of Fig. 2(a). These

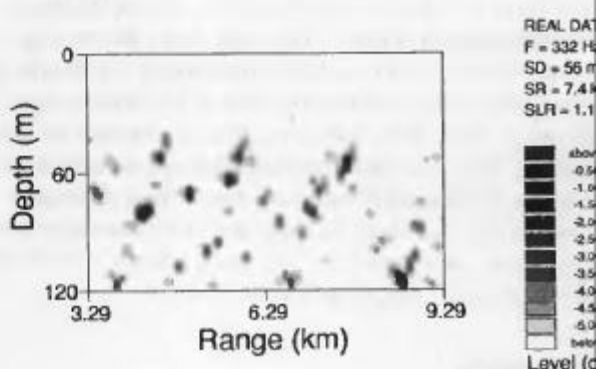


FIG. 7. Range/depth ambiguity surface obtained with real data of Fig. 2(b) and in the scenario of Fig. 1 with bottom sound speed of 1700 m/s, instead of 1600 m/s.

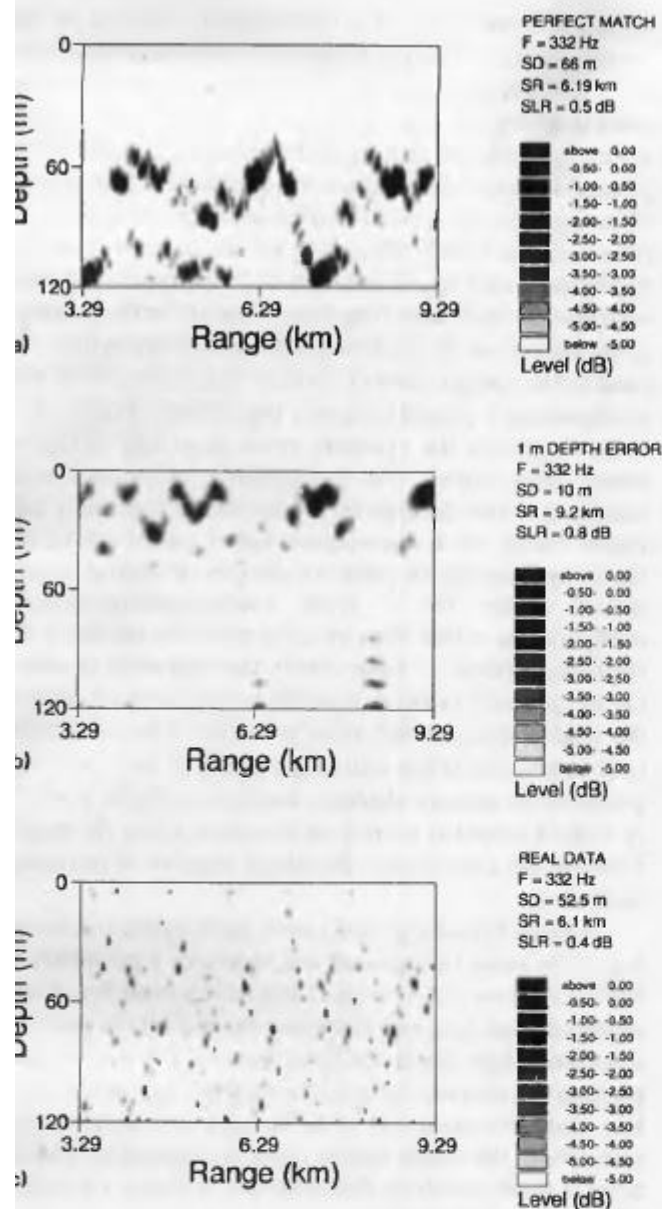


FIG. 8. Range/depth ambiguity surfaces obtained in the scenario of Fig. 1 with simulated data and true source depth/range of 61 m/6.29 km: with conventional matched-field processing (a), estimated source depth/range 6 m/6.19 km; 1-m array depth mismatch and normal-mode matching (b), estimated source depth/range 10 m/9.2 km. (c) shows the range/depth ambiguity surface obtained with conventional matched-field processing on the real data set of Fig. 2(b) and in scenario of Fig. 1. Expected source depth/range is 61 m/6.29 km, estimated 52.5 m/6.1 km.

lobes, found almost continuously during that 20-min run, are responsible for a number of losses of source localizations and may be due to sensor position errors which induce mode estimation inaccuracies. The higher-order modes and those with the lowest signal-to-noise ratio are the most sensitive to these errors. The relatively short range (5–7 km) implies that these modes still carry a non-negligible quantity of source location information needed for the range/depth localization process. This is apparently not the case shown in Fig. 3. The longer range (12 km) attenuates the higher-order

depth match, enhancing the source localization by reducing the sidelobes at shallow depths [Fig. 3(b)].

Tests done with the real data record [Fig. 2(b)] where the array has been raised by 1 or 2 m with respect to the assumed array depth of 40 m, and/or tilted by a few degrees showed that the sidelobe structure above the thermocline could be, in some cases, enhanced. In these cases, the source location was lost or ambiguous with a very low sidelobe rejection. This raises the question: How sensitive are matched-field techniques to errors on the sensor location? From synthetic data studies,<sup>15,16</sup> it was deduced that both normal-mode matching and the matched-field processor have equivalent sensitivity to sensor position mismatch. The sensitivity is claimed to be of the order of one wavelength accuracy in sensor depth and about 0.5 deg of tilt, for an array spanning the total water column. In our case, where the array spans only half the water column, one may expect higher sensitivity. This is illustrated by first showing with simulated data [Fig. 8(a)], the range/depth ambiguity surface obtained by matched-field processing in the same source/receiver environment used for Fig. 2. The source is estimated roughly at the correct location (66-m depth, 6.1 km range) with, however, a large ambiguity (sidelobe rejection 0.5 dB; localization accuracy  $\pm 11$  m in depth,  $\pm 0.1$  km in range). If the replica field is generated for an array raised by 1 m, the result using normal-mode matching is a loss of the source location [Fig. 8(b)] while with the matched-field processor the result is still poor but very close to that obtained in the perfect match case of Fig. 8(a). In other words with short arrays, a conventional matched field is more robust than normal-mode matching to sensor depth mismatch. This result can be easily understood by noting that the main difference between the two processors concerns the number of modes that can effectively be resolved in a given situation. The influence of sensor depth errors on mode estimation is higher for the highest-order modes. In a short-array configuration, this penalizes normal-mode matching when compared to conventional matched field. This is confirmed by looking at the matched-field result obtained from the real data record of Fig. 2, shown in Fig. 8(c). This range/depth ambiguity surface is consistent with that of Fig. 2(b) (sidelobes at shallow depths) with, however, poorer localization (sidelobe rejection of 0.4 dB and source location estimate 52.5-m depth, 6.1-km range). The effect of an horizontal sensor displacement degrades in the same manner for both processors. To some extent, the uncertainty of sensor position can be taken into account on both processors by introducing the appropriate correction factors for range and depth.

A few other remarks can be made when comparing normal-mode matching results presented here and those obtained with conventional matched-field on the same real data set.<sup>4</sup> In general, the localizations obtained with conventional matched-field are poorly defined, i.e., small resolution both in depth and range as well as poor sidelobe rejection typically 0.3 dB, compared to 1 or 1.5 dB with normal-mode matching. However, with a conventional matched field source results have been shown for the highest frequency (738 Hz



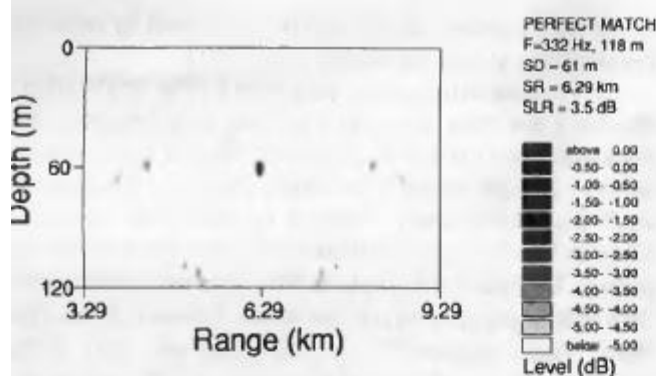


FIG. 9. Range/depth ambiguity surface obtained from simulated data on environmental conditions of Fig. 1 but with a 118-m-long array. True source location 61 m/6.29 km. This result was obtained either by normal-mode matching or conventional matched-field processing.

occasional and poor results could be obtained with normal-mode matching under similar conditions. This performance of the conventional matched-field processor is certainly due to its robustness to errors in the sensor location a particularly important concern both for shallow sources (in our particular environment) and for high frequencies. The main limitation of a conventional matched field is the small number of modes that can be resolved. This number depends essentially on the configuration of the receiving system, i.e., the effective aperture of the array relative to the acoustic channel in which the source energy propagates. To illustrate this point, we deviate from the receiving array structure of the real data study in order to simulate a 118-m array that spans the total water column (60 hydrophones at 2-m spacing). Figure 9 shows that the result is, as expected, identical for both processors and shows approximately the same performance as that obtained with normal-mode matching in the 62-m-long array case [Fig. 2(a)]. This result shows that the normal-mode matching, unlike the conventional matched field, takes into account the effective aperture and geometry of the array in the range/depth match process and adapts to it [see Eq. (9) and related remarks]. This feature is particularly important in shallow-water environments where the sound wave strongly interacts with the bottom, and therefore leaks a large amount of energy.

#### IV. CONCLUSION AND PERSPECTIVES

The performance of the normal-mode matching source localization method has been analyzed through a real data study. The two main issues for performance characterization are the sidelobe behavior of the range/depth ambiguity surface and the robustness of the method to environmental and source/receiver parameters mismatch. The dependence of the method on the precise knowledge of the receiving system geometry has also been studied. A comparison has been made with results obtained by the conventional matched field in the same conditions.

The results obtained with real data confirm the ability of normal-mode matching to handle short vertical arrays. Compared with the real data results obtained by matched-

sulting in some cases in a unambiguous estimate of source position. However, a relatively high sensitivity to sensor position and/or noise has been noticed, leading in some cases to ambiguous and/or inaccurate source location estimates. It is believed that normal-mode matching is less dependent than the conventional matched field on the number of modes that significantly contribute to the acoustic field; therefore, it is weakly affected by known changes in the environmental and source parameters;<sup>15</sup> the results obtained with normal-mode matching mainly depend on the accuracy of the normal-mode amplitude estimates which, in turn, depend on the configuration of the receiving system. When the configuration is precisely known, the method adapts to it in order to achieve the optimum result according to the summed data model. The performance of normal-mode matching mainly depends on the number of accurately estimated modes. As a consequence, better results can be obtained by selecting an optimum number of accurately estimated modes for a given source-medium-receiver configuration, rather than by using all of the modes in the matching process. To some extent, the suggestion of selecting an optimum number of modes is reinforced by some of the results obtained with real data where detections could only be obtained when matching a subset of the modes supported by the acoustic channel. Another possibility would be to make a weighted normal-mode match where the weighting function was a monotonic decreasing function of increasing mode order.

A better knowledge of the array position and the modeling of the noise background will represent a possibility to further improve the robustness and detection ability of normal-mode matching and therefore, its reliability in practical situations where the model describes well the real physical propagation characteristics of the medium. In practical shallow-water situations, due to the strong bottom-sound wave interaction, the sound field is often undersampled making normal-mode matching the technique of choice for range/depth source localization.

#### ACKNOWLEDGMENTS

Thanks are due to Dr. R. D. Hollett, who was responsible for the at-sea data collection, and to S. Bongi, who developed all the plotting software used in this paper.

- H. P. Buckner, "Use of calculated sound fields and matched-field detection to locate sound sources in shallow water," *J. Acoust. Soc. Am.* **59**, 3373 (1976).
- R. Klemm, "Range and depth estimation by line arrays in shallow water," *Signal Process.* **3**, 333-344 (1981).
- E. J. Sullivan, "Passive localization using propagation mode matching," *SACLANTCEN SR-117* [AD A189404], La Spezia, Italy, SACLA Undersea Research Centre (1987).
- R. M. Hamson and R. M. Heitmeyer, "Environmental and system effects on source localization in shallow water by the matched-field processing of a vertical array," *J. Acoust. Soc. Am.* **86**, 1950-1959 (1989).
- G. B. Smith, C. Feuille, D. R. DelBalzo, and C. L. Byrne, "A nonlinear matched-field processor for detection and localization of a quiet source in a noisy shallow-water environment," *J. Acoust. Soc. Am.* **85**, 1158-1168 (1989).
- E. C. Shang, "Source depth estimation in waveguides," *J. Acoust.*

ing in waveguides by using mode filter," *J. Acoust. Soc. Am.* **78**, 172-175 (1985).

[7] C. Yang, "A method of range and depth estimation by modal decomposition," *J. Acoust. Soc. Am.* **82**, 1736-1745 (1987).

[8] R. Wilson, R. A. Koch, and P. J. Vidmar, "Matched mode localization," *J. Acoust. Soc. Am.* **84**, 310-320 (1988).

[9] E. C. Shang, "An efficient high-resolution method of source localization processing in mode space," *J. Acoust. Soc. Am.* **86**, 1960-1964 (1989).

[10] L. Tolstoy and C. S. Clay, *Ocean Acoustics* (McGraw-Hill, New York, 1966).

[11] F. B. Jensen and M. C. Ferla, "SNAP: The SACLANCEN normal-mode acoustic propagation model," SACLANCEN SM-121 [AD A067256], La Spezia, Italy, SACLANCEN Undersea Research Centre (1979).

[12] G. Strang, *Linear Algebra and its Applications* (Academic, New York,

1976).

[13] F. B. Jensen, "Comparison of transmission loss data for different shallow water areas with theoretical results provided by a three-fluid normal mode propagation model," SACLANCEN CP-14 [AD A004805], La Spezia, Italy, SACLANCEN Undersea Research Centre (1974).

[14] S. M. Jesus, "Source localization in shallow water by normal mode matching: synthetic and real data analysis," SACLANCEN SR-1 [AD B140556], La Spezia, Italy, SACLANCEN Undersea Research Centre (1989).

[15] R. M. Hamson and R. M. Heitmeyer, "An analytical study of the effect of environmental and system parameters on source localization in shallow water by matched field processing of a vertical array," SACLANCEN SR-140 [AD B134955], La Spezia, Italy, SACLANCEN Undersea Research Centre (1988).